T.1: Unlocking the infrared frontier: Development of IR-FEL user facilities

L.S. Sharath Chandra, Shilpam Sharma, Ashish Khandelwal, Anudeep Singh and M. K. Chattopadhyay*

Free Electron Laser & Utilization Section
**Email: maulindu@rrcat.gov.in*

Abstract

The Raja Ramanna Centre for Advanced Technology (RRCAT), Indore houses a Free Electron Laser (FEL) developed in-house to lase in the wavelength region 12-50 μm, where the conventional sources fail to deliver a reasonable power. This region of electromagnetic spectrum is suitable for the study of resonant absorption of optical phonons, defects in semiconductors, non-linear dynamics, plasma resonances, low dimensional materials, polymers and their composites, etc. At present, macropulses of light coming from this FEL with a pulse repetition rate (PRR) 1-4 Hz and CW average power in excess of 5 mW (at 2 Hz PRR), with each macropulse consisting of about 200 micropulses of width 10 ps and separation about 33 ns, is available at the user laboratory for doing experiments. In the user laboratory, a Michelson interferometer has been developed to determine the wavelength of the FEL radiation. An infrared imaging set up has been developed to visualize the variation in the refractive index over the sample volume. The tunability of the FEL allows mode-selective imaging of samples for chemical finger printing within a solid. The pulsed nature of the FEL radiation can be utilized to perform time dependant experiments. In this article, the progress made in this direction is highlighted.

1. Introduction

Studies on the material properties in the mid and far infrared (IR) regions of the electromagnetic spectrum for wavelengths greater than 10 μm has been limited due to the lack of powerful sources. In this region of the electromagnetic spectrum, most of the commonly used materials either completely absorb the radiation through the n-phonon processes and/or optical phonon modes as in the case of non-metals, or completely reflect the radiation as in the case of metals. Over the past few decades, the development of FELs [1-3] and Synchrotron Radiation Sources (SRSs) delivering bright radiation in the IR regime has stimulated newer interest to unravel the novel properties in the fields of physics, materials science, chemistry, biology and medical sciences [4-8]. Several materials, e.g., the small gap semiconductors, polymers, low dimensional materials such as 2D-quantum materials and heterostructures are being explored both for photonic applications [9-12] and for their novel properties [13-17]. The refractive index of many of such materials in this wavelength range is quite large, which gives the scope for understanding the defect structure in the semiconductors and insulators. The FELs are the brightest sources for IR radiation with the added advantages of tunability of wavelength and ultra short pulse width. In this article, the experimental stations developed or being developed to study materials using the IR-FEL in RRCAT is presented.

2. Overview of FEL based IR sources

Conventional sources such as the black body or mercury arc lamp, radiate largely in the IR regime. These sources are widely used for spectroscopy experiments. Due to the lack of brightness, these sources offer a low signal to noise ratio [18], hindering, for example, the microscopic imaging at IR wavelengths. The SRSs offer white radiation at about three orders of magnitude higher brightness as compared to the conventional sources. In this case, the radiation is diffraction limited indicating that the spatial resolution can reach down to the size of the wavelength [18]. The IRFELs on the other hand, provide pulsed radiation with a pulse width down to a few ps at about three orders of magnitude higher brightness as compared to the SRSs. This allows a higher spatial resolution, beyond the diffraction limit [18]. Only a handful of such facilities are known to be available around the world, e.g, the FELIX in the Netherlands, FHI-FEL and FELBE in Germany, the Novosibirsk FEL in Russia, CLIO in France, FELiChEM in China, etc. [19]. In India, RRCAT is the first institute to develop a FEL working in the IR region, and it lases in the wavelength region 12-50 μm [19].

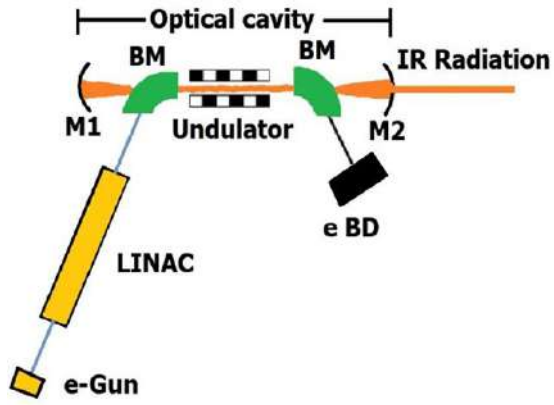

Fig. T.1.1: Schematic of an infrared free electron laser. e-Gun: electron gun; LINAC: linear accelerator; BM: bending magnet; M1, M2: mirrors; e BD: electron beam dump.

The schematic of an IRFEL is shown in Fig. T.1.1. The free electrons are generated using an electron gun (e-Gun) which is either a thermionic gun or a photo cathode gun [20, 21]. Then the free electrons in bunches are accelerated using a linear accelerator (LINAC) to about 10-30 MeV. Using bending magnets, these high energy electrons are made to pass through an undulator in which a series of alternating permanent magnets are placed. The electrons wiggle through these magnets due to the Lorentz force which alters their

velocity. The change in the velocity of the electrons results in the spontaneous emission of IR radiation. In order to achieve the coherence or the lasing action, an optical cavity using one 100% reflecting mirror (M1) and a partially reflecting (~90%) mirror are introduced across the undulator. The length of the cavity is adjusted such that the incoming second electron bunch is in phase with the back-reflected radiation emitted from the first bunch. At the exit of the undulator, another bending magnet is used to take out the electrons from the optical path to dump them in a multilayered target (e BD). Details of the relation between the undulator parameter and the emitted radiation can be found in ref. [19].

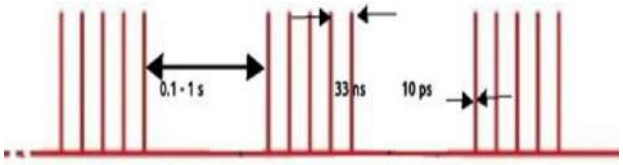

Fig. T.1.2: Pulse structure of an infrared free electron laser. Bunches of pulses are emitted at typically 1-10 Hz PRR.

Figure T.1.2 shows the typical pulse structure of the IR radiation emitted from an FEL. Due to the bunching of electrons in the LINAC and micro-bunching due to the interaction of the electric field of the wiggling elections bunches with that of the IR radiation inside the optical cavity, the IR output of the FEL consists of a series of bunches of pulses (macropulses) at 1-10 Hz PRR. Each macropulse thus consists of several micropulses of IR radiation.

3. Details of the IR-FEL functional at RRCAT

Figure T.1.3 shows the photograph of the IR-FEL developed at RRCAT [22]. The free electrons are accelerated to 18-25 MeV using a LINAC before feeding it to the undulator. The micropulse repetition rate can be selected between 29.75 MHz, 59.5 MHz or 119 MHz. The macropulse duration is 4-6 μs at present, with a PRR 1-4 Hz. The undulator for this FEL consists of 50 periods along its length, with a period length of 50 mm. The gap between the upper and lower jaws of the undulator can be varied between 27-40 mm [22] to vary the undulator parameter K_u from 1.2-0.5.

The wavelength of the radiation from the IR-FEL at RRCAT can be tuned in the wavelength range 12-50 μm by varying the undulator gap and the accelerated electron energy as shown in the Fig. T.1.4. It can be seen that two different electron energies viz., ~24 MeV and ~18 MeV are sufficient to cover the entire range of wavelengths. The brightness of the emitted radiation is in the range of 10^{14} photons/s/mm^2/mrad^2/0.1% BW which, for this wavelength range, is four orders of magnitude higher than the Indus SRS at RRCAT [23].

Fig. T.1.3: Photograph of the IR-FEL at RRCAT which lases at 12-50 μm.

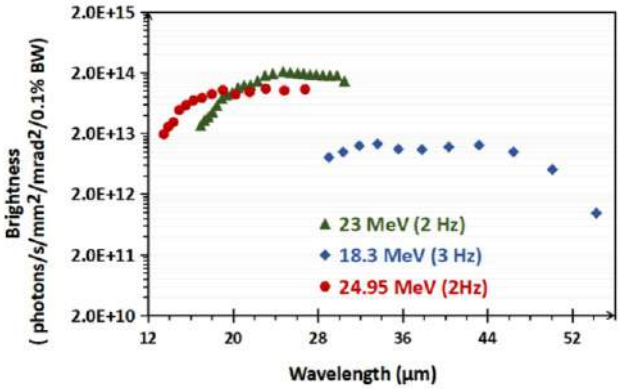

Fig. T.1.4: Brightness of IR-FEL radiation in the wavelength range 12-50 μm.

The stability of the radiation power over the duration of the user experiments has been ascertained by measuring the power delivered at the user laboratory over 6 hours. Figure T.1.5 shows this measured IR power at the user laboratory as a function of time. It is seen that the variation of power over 6 hours is less than 4% [23].

4. The IR-FEL beamline at RRCAT

The IR radiation emitted from a 3.5 mm aperture of the IR-FEL is transported over 60 m to the user laboratory through reflective optics (plane and spherical gold coated mirrors). A small portion of the beam is tapped at the exit port of the IR-FEL using a KRS beam splitter to measure the generated power. The beam lines are filled with dry nitrogen gas to avoid absorption due to atmospheric moisture. As shown in the Fig. T.1.6, six ports have been constructed for doing experiments using the radiation from the IR-FEL.

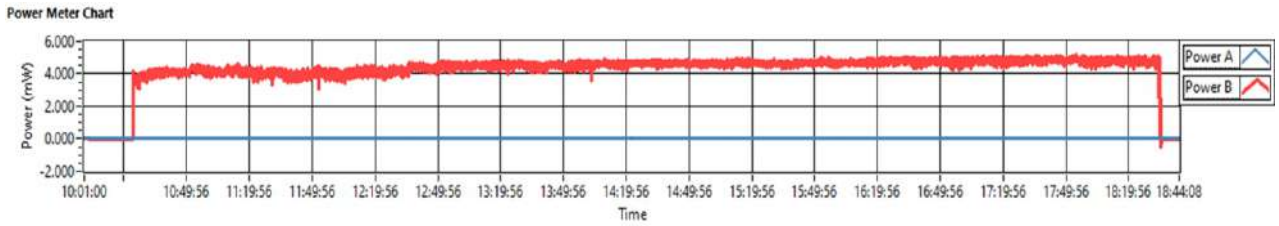

Fig. T.1.5: Stability of the radiation emitted from IR-FEL, as measured at the user laboratory.

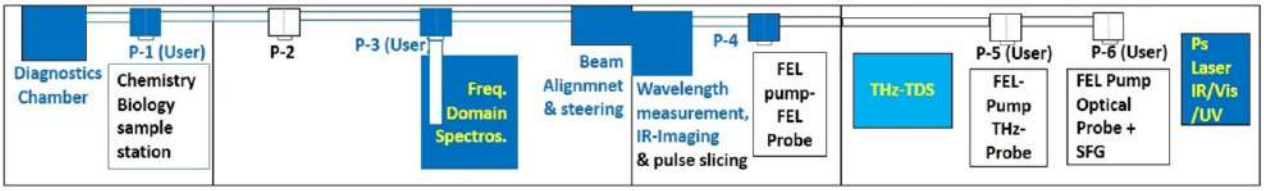

Fig. T.1.6: The IR beam line at the user laboratory rooms with exit ports. The blue colour indicates the facilities already in use.

5. Current and upcoming user facilities

A series of experimental platforms/stations are planned in the user laboratory. Some of them are completed, and are in use, while some of the others are under development, as discussed in the next subsections.

a. Michelson interferometer

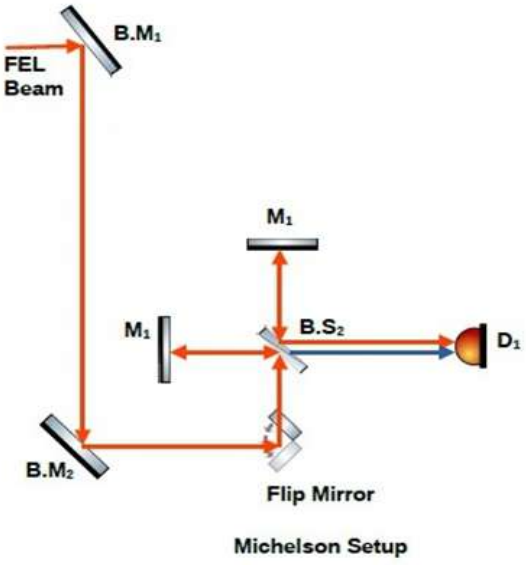

Fig. T.1.7: Schematic of the Michelson interferometer in the IR-FEL facility. B.M, M: Mirror; B.S: Beam splitter; D: detector.

An interferometer is an integral part of the optics laboratory where two beams of same source is made to superimpose to get the interference pattern. It is used to determine the spectral components of a white light source, as used for Fourier transform infrared (FTIR) spectroscopy, microscopic surface irregularity studies, or even for detecting gravitational waves. Since, the FEL emits monochromatic radiation, an interferometer is useful to know the central wavelength, wavelength spread, coherence length and side bands if any etc.

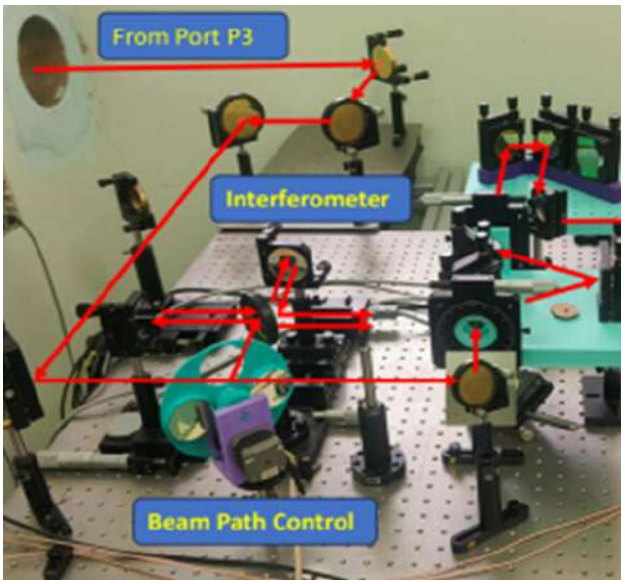

Fig. T.1.8: Michelson interferometer developed to characterize the IR-FEL radiation. Pyroelectric detectors are used for the detection of radiation. Double side polished high resistivity silicon is used as beam splitter. Gold coated copper mirrors are used as reflective optics.

One of the simplest interferometers to realize is the Michelson interferometer. Figure T.1.7 shows the schematic of the Michelson interferometer, where the mirrors M1 and M2 are

placed at equal distance from the beam splitter. One of the mirrors is moved in small steps over a specified length around the mean distance. By moving the mirror, a path difference is created between the two beams reflected by mirror M1 and M2 to introduce a phase difference between these two radiations leading to interference. The intensity of the IR beam is measured in small steps of the mirror movement. Figure T.1.8 shows the photograph of the Michelson interferometer developed to characterize the IR-FEL radiation. Pyroelectric detectors are used for the measurement of the wavelength of the radiation. Double side polished high resistivity silicon is used as beam splitter. Gold coated copper mirrors are used as reflective optics.

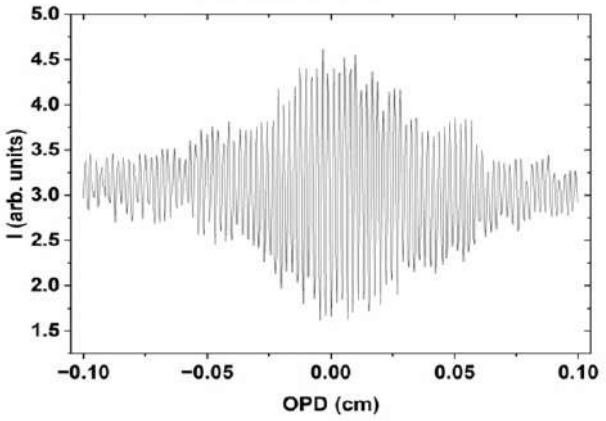

Fig. T.1.9: Interferogram from the IR-FEL radiation measured using Michelson interferometer.

The intensity as function of path difference is shown in Fig. T.1.9. The Fourier transform of the interferogram gives the IR-FEL light spectrum, which is shown in Fig. T.1.10. The central wavelength (λ) for this experiment is 22.26 μm. The full width at half maximum ($\Delta\lambda$) is 0.32 μm, which indicates the high monochromaticity of the IR-FEL light.

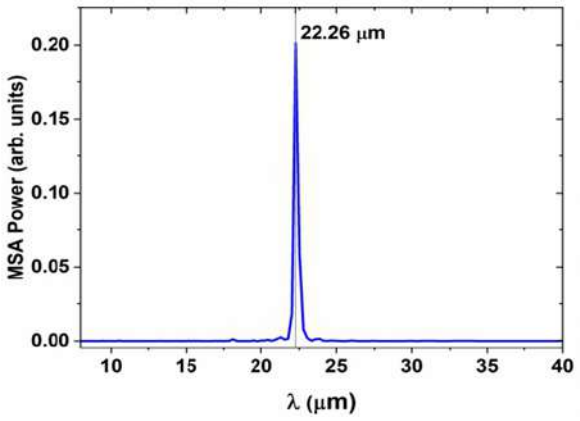

Fig. T.1.10: Fourier transform of the interferogram shown in Fig. T.1.9 showing a typical IR-FEL light spectrum that depicts its monochromaticity.

b. Temperature and magnetic field dependence in IR absorption spectroscopy

Non metallic solids often show strong broad band absorption in the 12-50 μm range, leading to poor signal to noise ratio in the transmission spectra measured in a FTIR spectrometer using conventional sources. Due to this, resonant transitions (if any) may be buried under the noise if the conventional sources are used. On the other hand, measurements under a pulsed magnet is impossible using a FTIR spectrometer. In such extreme conditions, radiation from FEL is valuable to study the novel properties of materials especially in the semiconductors and insulators [13, 14, 24].

Fig. T.1.11: Experimental set up used to measure the IR-FEL light absorption as a function of temperature and magnetic field.

Figure T.1.11 shows the photograph of the set up used for measuring IR absorption as a function of temperature and magnetic field using the radiation from the IR-FEL at RRCAT. The temperature of the sample can be varied from 300 K to 10 K in the presence of magnetic field up to 7 T using a cryogen free magnet cryostat system.

Fig. T.1.12: Photograph of the sample holder attached to the insert used for loading samples inside the cryostat shown in Fig. T.1.11.

Figure T.1.12 shows the sample mounting stage of the cryostat-insert used for measuring IR-FEL light absorption as a function of temperature and magnetic field. It consists of a copper plate with two circular apertures for mounting the sample and the reference. The reference for the bulk samples is the blank aperture. In the case of thin films, an identical

substrate is used as the reference. A silicon beam splitter is used for dividing the IR radiation into the reference beam and the probe beam. A pyroelectric detector is used to measure the intensity of the incident radiation (reference detector). Another pyroelectric detector is used to measure the transmitted radiation through the sample as well as the through the reference aperture (sample signal detector). A stepper motor is used for moving the sample and the reference aperture across the beam path inside the cryostat. The transmittance is estimated as the ratio of intensities of transmitted radiation through the sample to that transmitted through the reference aperture. Before finding this ratio, both the intensities are normalised to the incident power.

V_2O_3 is a classic material studied over decades [25]. It undergoes a metal to an insulator transition (MIT) along with a structural transition when the temperature is decreased below 150 K [26]. It was observed that the MIT can also be tuned with pressure, composition, electric field and photon energy [27-30]. Figure T.1.13(a) shows the temperature dependence of electrical resistance across the MIT. The thermal hysteresis (between warming and cooling runs) near 150 K indicates that the transition is of first order.

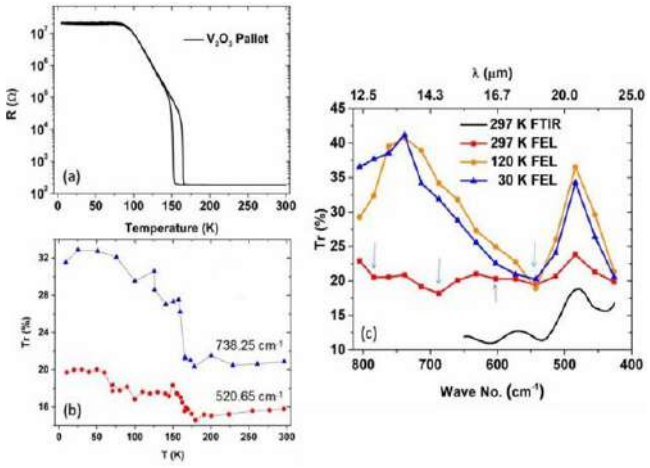

Fig. T.1.13: (a)Temperature dependence of electrical resistivity of V_2O_3. A first-order high temperature metal to low temperature insulator transition is observed near 150 K. (b) Transmission of IR-FEL light at 520.65 cm^{-1} and 738.25 cm^{-1} wave numbers through bulk V_2O_3 as a function of temperature. (c) Transmission spectra of bulk V_2O_3 as a function of wavelength (wave number) at different temperatures. For comparison, the data from FTIR spectroscopy are also plotted.

Figure T.1.13(b) shows the temperature dependence of transmittance at 520.65 cm^{-1} and 738.25 cm^{-1}. At both the frequencies, the transmittance changes across the MIT. However, the changes are minimal around 520.65 cm^{-1} and much larger near 738.25 cm^{-1} as the mode near the latter wave number is strongly dependent on temperature while that near the former wave number is not. This temperature dependence of the modes is clearly seen in Fig. T.1.13(c). The transmittance curve(s) in Fig. T.1.13(b), however, nearly mimic the temperature dependence of electrical resistivity as expected.

Figure T.1.13(c) shows the frequency dependence of IR-FEL light transmission at different temperatures. For comparison, the data obtained from the conventional FTIR spectrometer is also shown. One can observe that the transmission at a given frequency is higher for the FEL radiation in comparison with that measured using conventional FTIR spectrometer. This may be due to the interaction of the high electric field of the IR-FEL radiation with the sample. The high electric field may induce partial phase transformation to the insulating phase, or it may also induce nonlinear effects in the sample. Further studies are required to ascertain the origin of the excess transmission of FEL radiation. In this figure, various absorption modes are marked by arrows. As the temperature is decreased below the MIT, the transmittance increases due to the development of the insulating phase. These results suggest that in systems undergoing phase transitions, the temperature (and similarly magnetic field) dependence of transmittance can provide valuable information on their physical characteristics.

c. Infra-red imaging

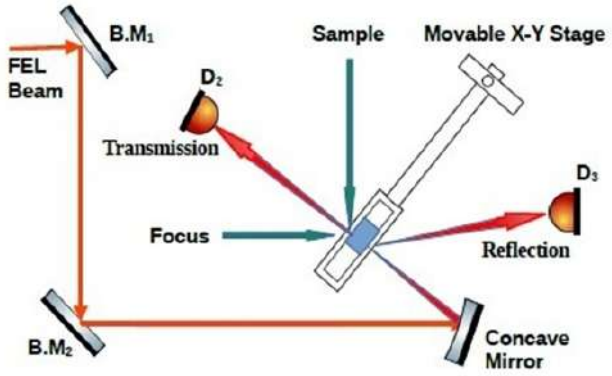

Fig. T.1.14: Schematic of the imaging set up. Images can be obtained both in the transmission and reflection modes.

Imaging using IR radiation is useful in studying composite materials. Use of FEL has two major advantages in imaging studies. (a) The brightness of the FEL light is several orders of magnitude higher than that of the conventional sources: this enhances the signal to noise ratio [18]. (b) The precise wavelength selectivity [31]: the wavelength can be tuned to specific characteristic excitations of the different compositions of the composites. For example, different pollutants present in soil [31], carbon-fibre reinforced polymers [10], interaction of reactive materials with a substrate [32], can be imaged to study the composition, defects, and/or reactions. Another advantage of imaging using IR-FEL light is that the materials that are opaque to the visible light, but transparent to IR radiation, can give

information about the microstructures buried inside the sample [33]. Keeping such applications in mind, an IR-FEL light based imaging facility has been developed in the user laboratory.

Figure T.1.14 shows the schematic of the imaging set up. The IR beam is focused on the sample using spherical concave/parabolic mirrors. The sample is scanned in X and Y direction using stepper motor controlled mechanical stages. The images can be obtained both in the transmission and reflection modes. The resolution of the image depends on how tightly one can focus the light. Figure T.1.15 shows the convergence of the IR-FEL light from a spot size of (a) 17 × 13 mm to (b) 0.8 × 1 mm.

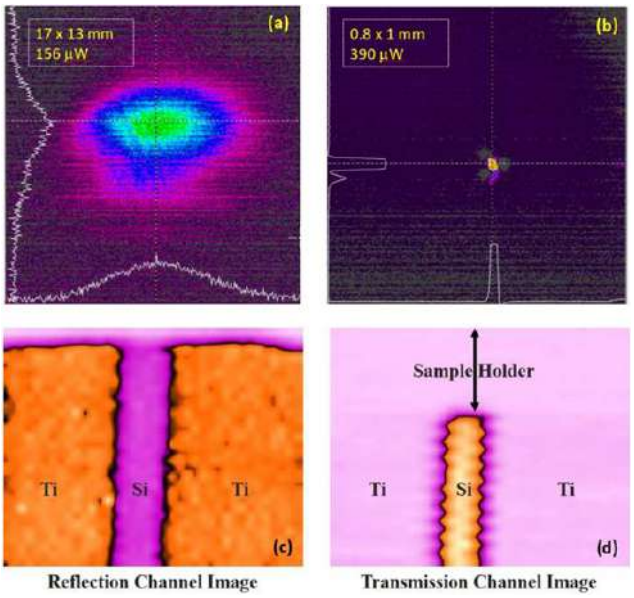

Fig. T.1.15: Focusing of the IR-FEL light from a spot size of (a) 17 × 13 mm to (b) 0.8 × 1 mm. (c) & (d) IR imaging of 100 nm thick, patterned Ti thin film on silicon substrate.

An example of imaging using this set up is shown in Fig. T.1.15. The sample under study is a 100 nm thick, patterned Ti thin film on silicon substrate. The image is obtained both in the (c) reflection and (d) transmission modes. Orange colour represents the maximum intensity measured, while pink represents the lowest measured intensity. A spatial resolution ~300 μm has been achieved in this set-up. The contrast seen in the panels (c) and (d) is due to the reflection of IR radiation from the free electrons within the Ti layer.

While the above-mentioned experimental facilities are already available for the users, more experimental stations are being developed for future use. In the following subsections, some of these activities are discussed.

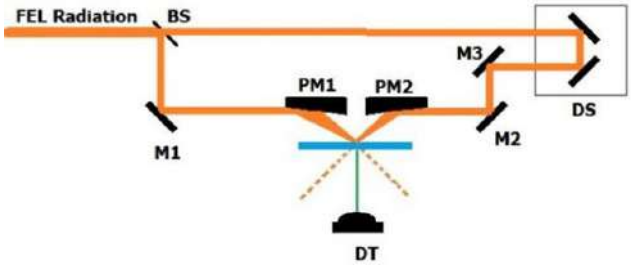

Fig. T.1.16: Schematic of the set up for second harmonic generation. BS: beam Splitter; M: Mirror; DS: Delay stage; PM: Parabolic mirror; DT: Detector; Blue rectangular slab: the sample.

d. Second harmonic generation using IR-FEL light

The high power of the IR-FEL can be used to explore the non-linear dynamics of small gap semiconductors and nano-structures [11, 12], e.g, CdSe, CdTe, ZnTe, Te, GaSe, $AgGaSe_2$, $AgGaTe_2$, $LiGaTe_2$, etc. Using second harmonic generation, CdTe may also be used in future as an autocorrelator device to study the IR-FEL pulse shape and thereby to tune the IR-FFL for increased monochromaticity. Figure T.1.16 shows the schematic of the set up required for second harmonic generation using a non-linear crystal (blue slab). The radiation is equally divided into two arms using a beam splitter such as high resistivity Si or a wire grid polarizer. A delay stage is attached to one of the arms. Both the beams are focused on the same location of the sample making equal angle to the normal of the sample. Both the beams are blocked after transmitting through the sample. The detector is placed at the plane normal to the radiation spot. The maximum intensity is obtained when the delay between two arms is zero. Such an experimental set up serves two purposes. Firstly, the nonlinear properties of new crystals can be studied, and secondly, it can be used to experimentally study the IR-FEL light pulse structure as stated above. The experimental set-up required for this is currently being built.

e. Pump-probe spectroscopy

A variation to the second harmonic set-up can be used to study the time evolution of a particular excitation [34-38] using the IR-FEL light. The measurements can be either one-colour [39-41] or two-colour [37, 41]. The choice of the method (one-colour or two-colour) and the energy of the pump beam is selected on the basis of the excitation to be studied. A relatively simple pump-probe set up being developed for the IR-FEL light is for FEL-pump FEL-probe spectroscopy (one-colour). In the case of two-colour pump-probe spectroscopy, a conventional pulsed laser and the IR-FEL need to be synchronized. This requires corrections for the phase error and very low timing jitters.

(i) IR-FEL-pump IR-FEL-probe spectroscopy

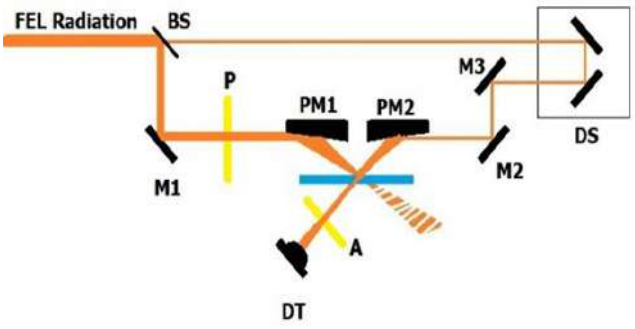

Fig. T.1.17: Schematic of the set up for FEL-pump FEL-probe spectroscopy. BS: beam Splitter; M: Mirror; DS: Delay stage; PM: Parabolic mirror; P: Polarizer; A: Analyser; DT: Detector; Blue rectangular slab: the sample;

Figure T.1.17 shows the schematic diagram of the one-colour pump-probe spectroscopy set up using the IR-FEL light. In this case most of the radiation (>90%) is used for pumping the sample, while a small amount of radiation (< 10%) is taped out using a beam splitter to probe the transmittance or reflectance from the sample as a function of the time delay between the probe beam and the pump beam incident on the sample. The set up is mostly ready, where qualifying experiments are currently being conducted.

(ii) IR-FEL-pump THz-probe spectroscopy

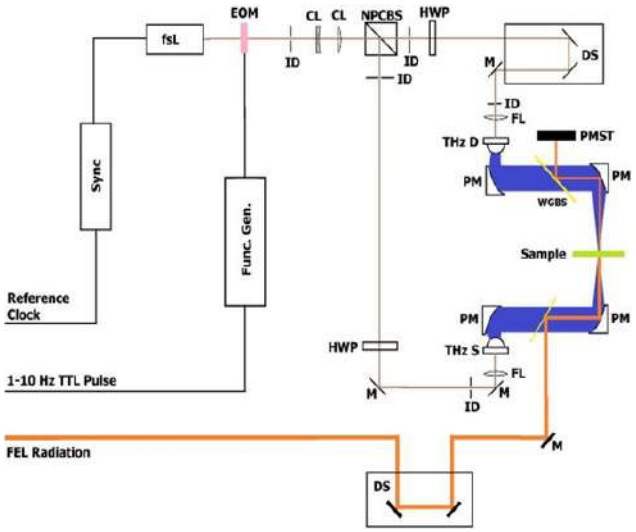

Fig. T.1.18: Schematic of the set up for IR-FEL-pump THz-probe spectroscopy. Sync: Synchronization (optoelectronic); fsL: femto second laser; Func. Gen: Arbitrary function generator; EOM: electro-optical modulator; ID: Iris disk; CL: collimating lens; NPCBS: non polarising cube beam splitter; HWP half wave plate; THz S: Terahertz source antenna; THz D: Terahertz detector antenna; PM: parabolic mirror; M: plane mirror; WGBS: wire grid beam splitter; PMST: Beam stopper.

Figure T.1.18 shows the schematic of the set up to be used for the IR-FEL-pump THz-probe experiments. This two-colour pump-probe spectroscopy requires the synchronization of a femto second laser (fsL) with the master clock of the FEL using optoelectronic synchronization system (Sync). The fsL light shall be used for THz (probe) generation and detection using antenna structures. Employing electro-optic modulation, a reference trigger pulse from the IR-FEL timing system shall be used to select a time window for THz generation and detection. Such a setup is presently being conceptualized at the IR-FEL user facility, and is expected to be developed by the end of 2029.

f. Photo-conductivity experiments using IR-FEL

The intense nature of the radiation from the IR-FEL can also be utilized to study the light induced electronic excitations in materials [13, 16]. In this case, the DC transient current will be measured as a function of time after irradiation with the IR-FEL light. In most of the cases, the induced current persists over few tens of μs or even up to a few seconds. Photoconductivity in the small gap semiconductors such as doped GaAs, doped Si and Ge, $Hg_{1-x}Cd_xTe$, $Pb_{1-x}Sn_xTe$, Kondo insulators such as SmB_6 and YbB_{12} have been studied using IR radiation from FEL sources [13, 16]. The photo-current is measured as a function temperature, magnetic field, wavelength and/or with respect to a specified time delay from the time of incidence of the radiation. In some samples such as graphene, transients may be quite fast so that the current may reach background levels within a few ps [17, 42]. Since, the decay of the photocurrent is fast, the current needs to be converted to voltage using a RF transimpedance amplifier and needs to be measured using a high-speed oscilloscope. A schematic of the required set-up is shown in Fig. T.1.19. This experimental set up is currently under development and will be available for measurements in near future.

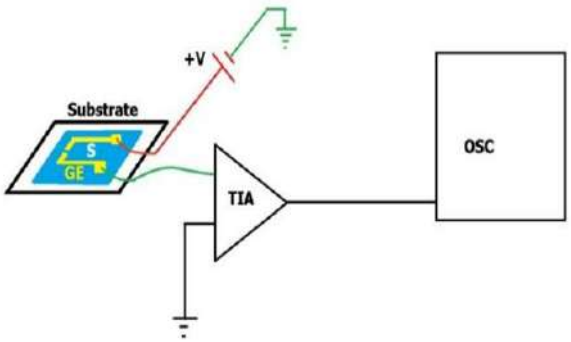

Fig. T.1.19: Schematic of the set up for the photo-conductivity experiments. S: Sample; GE: Gold contacts; TIA: RF Transimpedance Amplifier; OSC: Oscilloscope.

6. Conclusion

An IR-FEL lasing in the mid-far IR range (12-50 μm wavelength), is functional at RRCAT. Experimental measurements performed over more than six hours show that

the power stability of the IR-FEL radiation in the user laboratory is better than 4%. The wavelength characterization of this radiation has been performed using a Michelson interferometer developed in-house. A Single peak with less than 1.5% full width at half maximum has been observed, indicating the monochromaticity of the IR-FEL light. Two experimental stations developed and commissioned at the IR-FEL users facility have been used for studies by in-house as well as outside RRCAT users. A set up to measure the wavelength selective absorption/transmission as a function of temperature and magnetic field is in regular operation, and results of preliminary studies indicating photon induced excess transmission in V_2O_3 is presented. The features of the IR-FEL based imaging facility developed in-house to study composite materials for distinguishing differences in chemical composition, changes in the dielectric constant and for detecting buried layers of polymers opaque to visible radiation but transparent to IR have also been discussed. Several upcoming facilities such as second harmonic generation, time domain and photoconductivity measurement set ups are discussed in detail. With these developments, the IR-FEL establishment in RRCAT is shaping up into a unique experimental facility for research in different fields of science, including physics, materials science, chemistry and biology.

References

[1] B. N. Murdin, Contemporary Phys. 50, 391 (2009)

[2] J. E. Walsh, Proc. SPIE, 666, 22 (1986)

[3] C. A. Brau, Science 239, 1115 (1988)

[4] W. M. Dennis, J. Optical Soc. Ame. B 6, 1045 (1989)

[5] D. D. Dlott, and M. D. Fayer, IEEE J. Quanum Electron. 27, 2697 (1991)

[6] G. S. Edwards, S. J. Allen, R. F. Haglund, R. J. Nemanich, B. Redlich, J. D. Simon, and W. C. Yang, Photochem. Photobio. 81, 711 (2005)

[7] F. Vatansever, M. R. hamblin, Photonics Lasers med. 4, 255 (2012)

[8] T. Kawasaki, A. Nagase, K. Hayakawa, F. Teshima, K. Tanaka, H. Zen, F. Shishikura, N. Sei, T. Sakai, and Y. Hayakawa, ACS Omega 10, 13860 (2025)

[9] H. Chen, L. Gao, Z. Qin, Y. Ge, K. Khan, Y. Song, G. Xie, S. Xu, H. Zhang, Appl. Mater, Today 21, 100800 (2020)

[10] L. Senni, S. Laureti, M. K. Rizwan, P. Burrascano, D. A. Hutchins, L. A. J. Davis, and M. Ricci. NDT and E Inter. 102, 281 (2019)

[11] H. Zen, R. Hajima, and H. Ohgaki, Sci. Rep. 13, 6350 (2023)

[12] W. Schollkopf, S. Gewinner, H. Junkes, A. Paarmann, G. v. Helden, H. Bluem, A. M. M. Todd, Proc. SPIE, 9512, 95121L (2015)

[13] J. Kaminski, J. Spector, W. Pretti, and M. Weispfenning, Appl. Phys. Lett. 52, 233 (1988);

[14] A-L. Barra, M. Goiran, R. Sessoli, and S. A. Zvyagin, Comp. Ren. Phys. 14, 106 (2013);

[15] S. P. Horvath, J.-P. R. Wells, A. F. G. van der Meer, and M. F. Reid, Optical Mater. 66, 8 (2017);

[16] M. A. W. van Loon, N. Stavrias, N. H. Le, K. L. Litvinenko, P. T. Greenland, C. R. Pidgeon, K. Saeedi, B. Redlich, G. Aeppli, and B. N. Murdin, Nat. Photon. 12, 179 (2018);

[17] M. Mittendorff, J. Kamann, J. Eroms, D. Weiss, C. Drexler, S. D. Ganichev, J. Kerbusch, A. Erbe, R. J. Suess, T. E. Murphy, S. Chatterjee, K. Kolata, J. Ohser, J. C. K. Otto, H. Schneider, M. Helm, and S. Winnerl, Optics Express 23, 28728 (2015)

[18] T. I. Smith, Nucl. Instrum. Methods Phys. Res. A 483, 565 (2002)

[19] S. Chandran, R. S. Saini, S. Lal, T. Dave, B. Biswas, A. Kumar, U. Kale, S. K. Gupta, S. Sharma, A. Singh, K. K. Pant, V. Kumar, Nucl. Instrum. Methods Phys. Res. A 1084, 171214 (2026)

[20] S. Krishnagopal and Vinit Kumar, Rad. Phys. Chem. 70, 559 (2004)

[21] T. Asaka, H. Ego, H. Hanaki, T. Hara, T. Hasegawa, T. Hasegawa, T. Inagaki, T. Kobayashi, C. Kondo, H. Maesaka, S. Matsubara, S. Matsui, T. Ohshima, Y. Otake, T. Sakurai, S. Suzuki, Y. Tajiri, S. Tanaka, K. Togawa, and H. Tanaka, Phys. Rev. Accel. Beams 20, 080702 (2017)

[22] K. K. Pant, V. Kumar, B. Biswas, A. Kumar, S. Lal, S. Chandran, S. K. Gupta, Md. Khursheed, P. Nerpagar, A. K. Sarkar, R. K. Pandit, K. Ruwali, K. Sreeramulu, S. Das, R. S. Shinde, S. Chouksey, J. K. Parate, V. Bhanage, P. P. Deshpande, S. Tiwari, M. Joshi, L. Jain, A. Valecha, A. Pathak, M. A. Ali, H. R. Bundel, P. Shrivastava, T. Reghu, U. Kale, Y. Wanmode, P. Mohania, J. Mulchandani, A. Patel, M. Acharya, A. Mahawar, M. Lad, M. K. Jain, N. Tiwari, P. S. Bagduwal, V. G. Sathe, S. Joshi, R. Shiroman, A. S. Yadav, R. Kumar, A. Singh, V. K. Dwivedi, M. Borage, and S. R. Tiwari, Cur. Sci. 114, 367 (2018)

[23] M. K. Chattopadhyay, B. Biswas, S. Sharma, A. Khandelwal, S. Chandran, L. S. Sharath Chandra, T. Dave, R. S. Saini, S. Lal, A. Kumar, U. Kale, S. K. Gupta, R. K. Pandit, H. N. Sidam, P. Nerpagar, A. Chakraborty, R. K. Meena and K. K. Pant, Curr, Sci. 128, 710 (2025)

[24] C. J. G. M. Langerak, L. Li, L. Van Bockstal, A. Ardavan, M. J. van de Pol, A. F. G. van der Meer, F. Herlach, H. U. Mueller, R. J. Nicholas, and J. Singleton, Physica B 246-247, 400 (1998)

[25] S. Y. Kim, M.-C. Lee, G. Han, M. Kratochvilova, S. Yun, S. J. Moon, C. Sohn, Je-G. Park, C. Kim, and T. W. Noh, Adv. Mater. 30, 1704777 (2018)

[26] C. Huang, A. Rakshit, G. Janka, Z. Salman, A. Suter, T. Prokscha, B. A. Frandsen, and Y. Kalcheim Adv. Electron. Mater. 11, 2500028 (2025)

[27] I. Valmianski, J. G. Ramirez, C. Urban, X. Batlle, and I. K. Schuller, Phys. Rev. B 95, 155132 (2017)

[28] P. Homm, M. Meghini, J. W. Seo, S. Peters, and J. P. Locquet, APL Mater. 9, 021116 (2021)

[29] P. Hansmann, A. Toschi, G. Sangiovanni, T. Saha-Dasgupta, S. Lupi, M. Marsi, and K. Held, Phys. Status Solidi B 250, 1251 (2013)

[30] F. Giorgianni, J. Sakai, and S. Lupi, Nat. Commun. 10, 1159 (2019)

[31] Y. Cheng, H. sun, E. Yang, J. Lv, B. Wen, F. Sun, L. Luo and Z. Liu, J. Hazard. Mater. 411, 125129 (2021)

[32] S. G. Kazarian, and K. L. A. Chan, Macromolecules, 37, 579 (2004)

[33] D. M. Mittleman, Opt. Exp. 26, 9417 (2018)

[34] N. Mori, The Rev. Laser Engg. 31, 818 (2003)

[35] J. Kono, A. H. Chin, A. P. Mitchell, T. Takahashi, and H. Akiyama, Appl. Phys. Lett. 75, 1119 (1999)

[36] M. A. Zudov, A. P. Mitchell, A. H. Chin, and J. Kono, J. Appl. Phys. 94, 3271 (2003)

[37] G. A. Khodaparast, D. C. Larrabee, J. Kono, D. S. King, J. Kato, T. Slupinski, A. Oiwa, H. Munekata, G. D. Sanders, and C. J. Stanton, J. Appl. Phys. 93, 8286 (2003)

[38] G. A. Khodaparast, D. C. Larrabee, J. Kono, D. S. King, S. J. Chung, and M. B. Santos, Phys. Rev. B 67, 035307 (2003)

[39] M. Broquier, H. Dubost, R. Kolos, J. Lefevre, and A. Tramer, J. M. Ortega, J. M. Berset, A. Peremans, AIP Conf. Proc. 364, 154 (1996)

[40] H. A. Hafez, S. Kovalev, K.-J. Tielrooij, M. Bonn, M. Gensch, and D. Turchinovich, Adv. Optical Mater. 8, 1900771 (2020)

[41] S. P. Horvath, J.-P. R. Wells, A. F. G. van der Meer, and M. F. Reid, Optical Mater. 66, 8 (2017); J. M. Ortega, Nucl. Instrum. Methods Phys. Res. A 507, 8 (2003)

[42] M. Mittendorff, S. Winnerl, J. Kamann, J. Eroms, D. Weiss, H. Schneider, and M. Helm, Appl. Phys. Lett. 103, 021113 (2013)